Ti$_{Sr}$ antisite: an abundant point defect in SrTiO$_3$

Antti Karjalainen,[1,2] Vera Prozheeva,[2] Ilja Makkonen,[1] Christo Guguschev,[3] Toni Markurt,[3] Matthias Bickermann,[3] and Filip Tuomisto[1,2]

[1] *Department of Physics and Helsinki Institute of Physics, University of Helsinki, P.O. Box 43, FI-00014 Helsinki, Finland*

[2] *Department of Applied Physics, Aalto University, P.O. Box 15100, FI-00076 Espoo, Finland*

[3] *Leibniz-Institut fur Kristallzuchtung, Max-Born-Str. 2, 12489 Berlin, Germany*

(Dated: 6 June 2020)

We present a systematic study of the positron lifetime as a function of measurement temperature in SrTiO$_3$ single crystals grown in different conditions and by different synthesis methods. We combine our experimental results with state-of-the-art theoretical calculations of positron annihilation parameters. We find that the essentially omnipresent $180 - 190$ ps lifetime component is most likely the Ti$_{Sr}$ antisite defect, possibly coupled with one or more oxygen vacancies, supporting the importance of the Ti$_{Sr}$ antisite related defects in SrTiO$_3$.

1

I.   INTRODUCTION

Strontium titanate ($SrTiO_3$) is the prototype perovskite-structured complex oxide with a relatively wide band gap of 3.25 eV[1]. $SrTiO_3$ bulk crystals serve as substrates for growth of many complex oxides, while $SrTiO_3$-based thin film heterostructures have been the topic of intense study for the past two decades[2]. When materials synthesis reaches the level of quality where the the densities of extended defects are low enough not to affect the material properties in a significant manner, the attention is typically turned to point defects. In $SrTiO_3$, the main point defect of interest has been the O vacancy due to its abundance both at surfaces and in the bulk[2,3]. The phenomena related to point defects on the Sr and Ti sublattices have been studied much less, in particular from the point of view of their experimental characterization. Recently, some attention has been given to the Ti_{Sr} antisite related defects and their possible association with ferroelectricity in $SrTiO_3$[4–8].

Positron annihilation spectroscopy is a method that is particularly suitable for studying vacancy-type defects on the cation sublattice(s) in compound semiconductors[9]. In addition to vacancy-type defects, positrons are also sensitive to negatively charged defects without excess open volume, such as ionized acceptor impurities[9]. In some cases positrons have also been shown to be sensitive to small-size impurity atoms substituting for larger metal atoms, such as Li on Zn site in ZnO[10,11] or Be on Ga site in GaN[12]. A handful of papers has been published[13–21] on applying positron annihilation spectroscopy, in particular positron lifetime spectroscopy, to study vacancy-type defects in $SrTiO_3$. Defect-related positron lifetimes ranging from $\sim$170 ps to $\sim$320 ps have been reported in $SrTiO_3$, with values in the $180 - 190$ ps range being the most frequently observed[13–20]. The positron lifetimes of $\sim$180 ps and $\sim$280 ps have been associated with cation monovacancies, V_{Ti} and V_{Sr}, respectively, through direct comparison to positron lifetimes calculated with the atomic superposition method[13,16–20]. However, even when using the most recent theoretical methods, the predictive value of the calculated lifetimes on the absolute scale has room for improvement[22–24]. Instead, reliable comparison of experimental and theoretically calculated lifetimes is possible through the changes caused by defects relative to the positron lifetime in the perfect (defect-free) lattice, also called as the bulk positron lifetime. Unfortunately, the positron lifetime in $SrTiO_3$ lattice is still unresolved, with reported – mostly indirectly obtained – values scattered in a wide range from $\sim$135 ps to $\sim$160 ps[13,15,21], making the

experiment-theory comparison difficult.

In our work, we make an attempt at interpreting in detail the positron lifetimes measured in $SrTiO_3$ bulk crystals in terms of the most abundant defects detected by the positrons. To do this, we present a systematic study of the positron lifetime as a function of measurement temperature, crucial for resolving the effects of different charge states of the defects[9], in $SrTiO_3$ grown in different conditions and by different synthesis methods. We combine our experimental results with state-of-the-art theoretical calculations of positron annihilation parameters[25]. We find that the essentially omnipresent $180-190$ ps component is most likely the Ti_{Sr} antisite defect, possibly coupled with one or more oxygen vacancies, supporting the importance of the Ti_{Sr} antisite related defects in $SrTiO_3$[4–7]. Importantly, even with our systematic approach, this interpretation is unfortunately based on indirect evidence, calling for further investigations to resolve the question.

II.   METHODS

A.   Experimental

The $SrTiO_3$ single crystals were grown from the melt by using the Czochralski (Cz) and edge-defined film-fed growth (EFG) methods at temperatures of about 2350 K in slightly oxygen enriched argon atmospheres at atmospheric pressure[26]. The samples EFG-A1 and EFG-A2 were prepared from the same EFG crystal, where the O_2 concentration was continuously lowered (from 1550 to 2 ppm_v) during growth, so that for the samples denoted as EFG-A1 and EFG-A2 it was about 2 ppm_v and 450 ppm_v O_2, respectively. The oxygen concentration was measured at the gas outlet of the growth chamber by using a capillary coupled mass spectrometer. The samples EFG-B and EFG-C are from different growth runs, where the oxygen supply was constant and significantly higher (1550 ppm_v) than for the samples EFG-A1/2. The Czochralski sample Cz-D was grown at the highest oxygen concentration of about 1600 ppm_v. For all experiments (except for EFG-A1/2) the given oxygen concentrations correspond to the nominal compositions adjusted by mass flow controllers at the gas inlet to the growth chamber.

The positron lifetime in the samples was studied with a standard fast positron lifetime setup. The ^{22}Na positron source material was sealed in 3 µm thick Al foil and sandwiched

between two identical samples. The positron lifetime was measured with two scintillator-photomultiplier detectors with a Gaussian timing resolution of 250 ps (full width at half maximum). The measurements were performed as a function of sample temperature with the help of a closed-cycle He cryostat with a high-temperature interface. A total of 10^6 counts was accumulated at each measurement point. Positron annihilations in the source as well as positronium (400 ps, 2%; 210 ps, 3%; 1500 ps, 0.1-0.3 %) were subtracted from the spectra before analysis.[9]

The positron lifetime spectra were decomposed by fitting a sum of exponential lifetime components, $n(t) = \sum_i I_i \exp(-t/\tau_i)$, convoluted with the Gaussian resolution function. Positrons annihilate in the state i with intensity I_i and lifetime τ_i. A positron state i can either be a delocalised state in the lattice or a localised state trapped in a defect of open volume. The average lifetime $\tau_{\mathrm{ave}} = \sum_i \tau_i I_i$ is insensitive to fitting procedures, and it can be determined with an accuracy better than $1\,\mathrm{ps}$. If only one defect is significantly trapping positrons, the interpretation of the lifetime decomposition is relatively simple as the longer lifetime component corresponds the defect lifetime $\tau_2 = \tau_D$. Temperature-resolved experiments can detect charge states of vacancies due to temperature dependent positron trapping to charged defects. The trapping rate of a negatively charged vacancy enhances at low temperatures according to $T^{-1/2}$ whereas positively charged defects do not trap positrons. In this work, fitting more than two lifetime components to the experimental lifetime data did not produce statistically reliable results.

B. Theoretical calculations

The structure of cubic perovskite $SrTiO_3$ is shown in Fig. 1. Both cations have O atoms as their nearest neighbors. Ti has 6 O atoms as nearest neighbors whereas Sr has 12 O atoms. The Sr atoms have also longer distance to the neighboring O atoms by a factor of $\sqrt{2}$. We calculated the positron lifetime in $SrTiO_3$ lattice, antisites and cation monovacancies both with and without surrounding O vacancies and in cation divacancies complexed with O vacancies.

Positron states and annihilation in the $SrTiO_3$ lattice and its defects are modeled using the approach detailed in Ref. 22. We apply a cubic $3 \times 3 \times 3$ supercell with 135 atoms, and use the experimental lattice parameter of 3.905 Å. The electronic and ionic structures were

modeled using density functional theory within the local-density approximation[27] (LDA) and projector augmented-wave method[28] as implemented in the VASP code.[29–31] The repulsive forces on ions due to the localized positron were taken into account when considering trapped positrons.[22] Positron states and lifetimes were calculated using the LDA correlation potential and enhancement factor.[32]

Instead of performing fully self-consistent two-component calculations in which both the electron and positron densities are solved fully self-consistently, we assume in the case of both delocalized and trapped positron states that the positron density does not affect the average electron density and take the zero-positron density limits of the functionals. This scheme has been shown to give results that agree with more self-consistent modeling.[33] The LDA enhancement typically predicts too short lifetimes in comparison with the experiment but lifetime differences of defects relative to the lattice lifetime can be compared with high confidence.[10,22] On the other hand, the choice of the one-component exchange-correlation functional applied for electrons does not have much significance in this work. Positron annihilation characteristics, such as the lifetime, mainly depend on the predicted defect geometry. The positron is not sensitive to otherwise important properties such as the predicted electron energy band gap and the Ti d shell configuration in $SrTiO_3$ (the motivation why its density functional works often involve a Hubbard U term). The latter is due a compensation mechanism[34,35] in which the positron density follows any changes in the electron density, for example, due to an improved description. This keeps their mutual overlap, affecting the annihilation rate, constant.

III. RESULTS AND ANALYSIS

A. Experiments

Figure 2 shows the average positron lifetime τ_{ave} measured as a function of temperature in all 5 samples. The most prominent feature is that at low temperatures (below 150 K) the average positron lifetime converges to 185 ± 3 ps in all samples. At thigh temperatures the average positron lifetimes exhibit three different types of behavior.

Sample Cz-D. The average positron lifetime is constant 183 ps below 250-300 K. Above 300 K, the average positron lifetime decreases all the way to 165 ps at 600 K. Below 300 K,
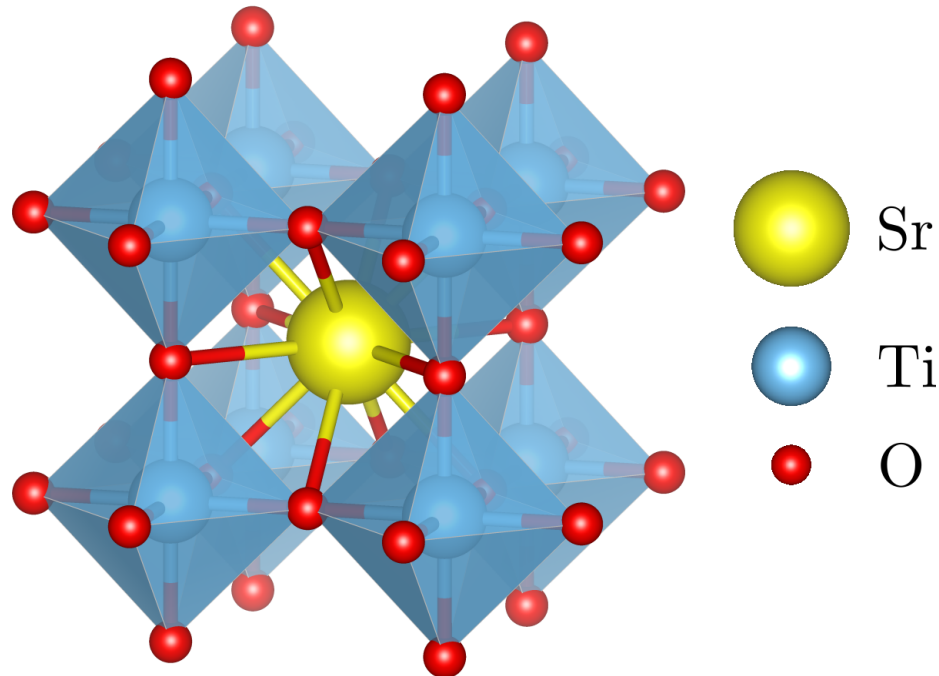
FIG. 1. The cubic perovskite structure of $SrTiO_3$ (Ref. 36). Sr has 12 O atoms as nearest neighbors, and Ti has 6 O atoms.

the lifetime decomposition shows only a single lifetime component. At temperatures 300-600 K, a second lifetime component emerges. However, the statistical uncertainty (standard deviation) of the lifetime decomposition is significant (average $\tau_2 = 220 \pm 40$ ps, $I_2 = 15 \pm 10$ %). Hence, we do not show the fitted components nor do we analyze them in more detail.

Samples EFG-A1 and EFG-A2. Figure 3 shows the average positron lifetime as well as the two fitted components as a function of measurement temperature in the samples EFG-A1 and EFG-A2. The average positron lifetime, τ_{ave}, increases with temperature above 150-200 K. The two samples have the same constant average lifetime of 185 ps below 150 K. The average lifetimes differ slightly at high temperatures, with the largest difference at 600 K being 7 ps. Two lifetime components can be resolved above 250 K and the intensity I_2 of the second lifetime component τ_2 increases from zero to $30 - 35$ % at 600 K. The second lifetime component is constant $\tau_2 = 320 \pm 20$ ps and the statistical error estimate of the fitting procedure decreases with the increasing intensity of the component. The value of first lifetime component, τ_1, coincides with τ_{ave} at 250 K and decreases with the increase of I_2.
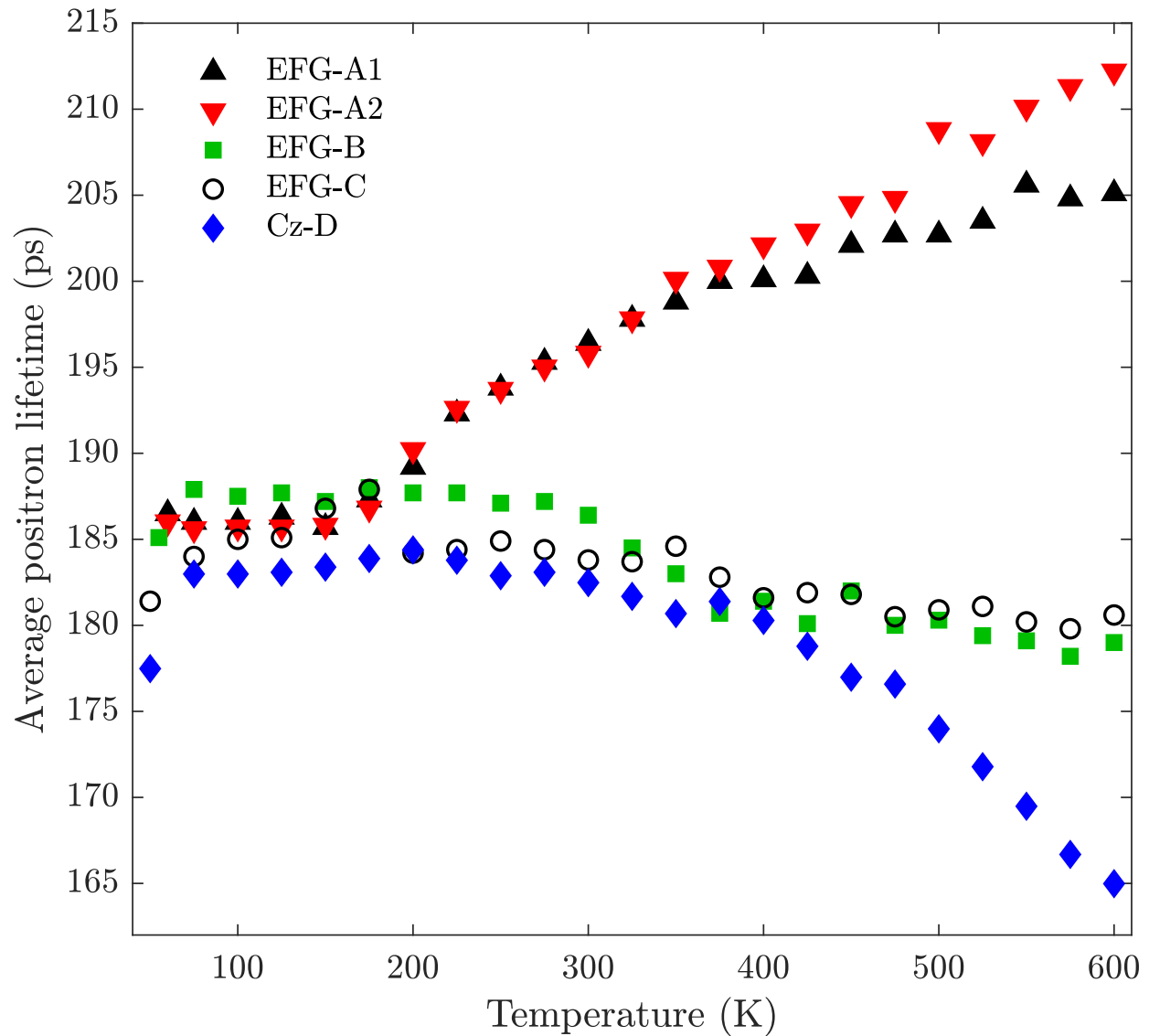
FIG. 2. The average positron lifetime τ_{ave} measured in the SrTiO$_3$ samples as a function of temperature.

Samples EFG-B and EFG-C. Figure 4 shows the average positron lifetime as well as the two fitted components as a function of measurement temperature in the samples EFG-B and EFG-C. The average positron lifetime decreases with increasing temperature above 300 K, but clearly less than in sample Cz-D. The lifetime decomposition succeeds above $200 - 300$ K. The second lifetime component τ_2 in sample EFG-B has a roughly constant value of 255 ± 15 ps for whole the temperature range. For EFG-C, the second lifetime component increases with temperature: roughly constant and similar to τ_2 in EFG-B up to 450 K, and
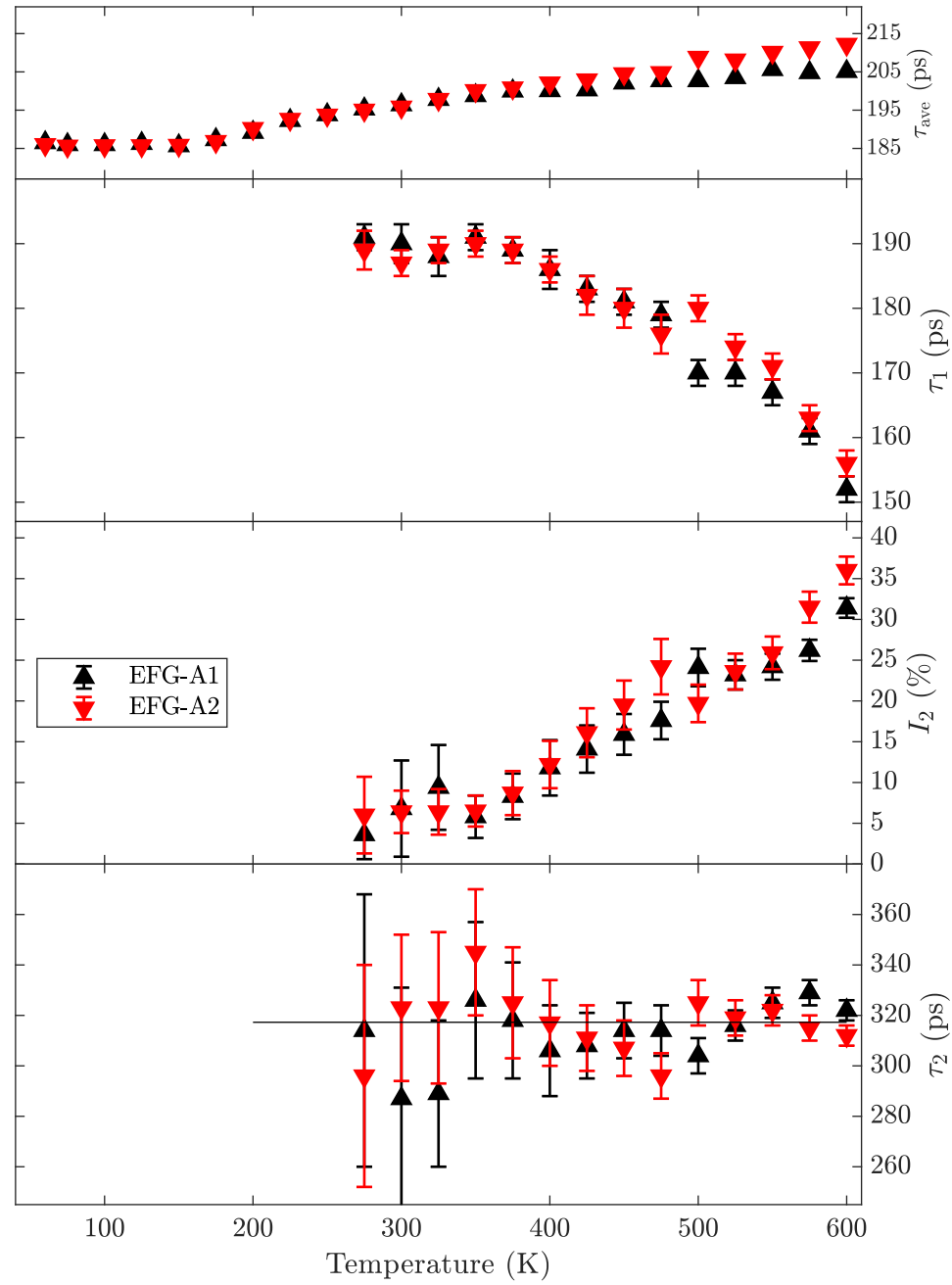
FIG. 3. The average lifetimes τ_{ave}, the decomposed lifetime components τ_1 and τ_2, and the intensity of the second component I_2 in samples EFG-A1 and EFG-A2. The intensity of the first component is $1 - I_2$. An error weighted average of the τ_2 in both samples is also shown $\tau = 320 \pm 20\,\mathrm{ps}$.

above 400 K, increasing up to 340 ps at 600 K. For the sample EFG-B, the intensity of the second lifetime component I_2 emerges at 300 K and increases to 35 % at 400 K. Above 400 K, and decreases steadily down to 20 % at 600K. The values of I_2 in sample EFG-C scatter around a constant value of roughly 35 % between 200 K and 400 K. Above 400 K, I_2 in EFG-C also decreases steadily but with a steeper slope, down to 10 % at 600 K. The different trends in intensity I_2 and the value of the second lifetime component τ_2 in samples EFG-B and EFG-C compensate each other in such a way that the average positron lifetimes in both samples have similar values above 400 K. The behavior of the first lifetime component τ_1 in both samples is opposite to I_2.

B. Theoretical calculations

The calculations show that V_O does not trap positrons, similarly as the Sr_{Ti} antisite also when neighbored by an oxygen vacancy. Instead, the Ti_{Sr} antisite traps positrons in spite of the relatively small associated open volume. It should be noted that theoretical calculations predict two stable configurations for the Ti_{Sr} antisite, both off-center, labeled [100] (ground state) and [110] (metastable state) based on the direction of the relaxation.[5] The calculated positron lifetimes are shown in Table I. The positron lifetime in $SrTiO_3$ lattice is 128 ps. For historical naming reasons, we denote positron lifetime in the lattice as τ_B where "B" stands for "bulk". The shortest positron defect lifetime was found in Ti_{Sr} in the off-center [100] configuration (τ_B + 32 ps). The positron lifetime in the larger cation vacancy (V_{Sr}) is expectedly longer (τ_B + 105 ps) than in V_{Ti} (τ_B + 44 ps).

As Sr has a larger a number of neighboring O atoms than Ti, and the Sr-O distance is larger than the Ti-O distance, the Sr vacancy lifetime is less sensitive to the number of neighboring V_O than the lifetime in V_{Ti}-nV_O. The V_{Sr}, V_{Sr}-V_O and V_{Sr}-$2V_O$ are essentially indistinguishable, and even adding 6 V_O to V_{Sr} only increases the vacancy lifetime by 30 ps. Interestingly, the same applies to the Ti_{Sr} antisite. Even when comparing Ti_{Sr} [110] and Ti_{Sr}-V_O [$\bar{1}\bar{1}0$] configurations[6] where the effect of the additional neighboring O vacancy is expected to be the largest, the positron lifetime hardly changes (τ_B + 40ps). In contrast, already adding one V_O to V_{Ti} extends the lifetime by almost 20 ps, and each additional V_O strongly increases the lifetime, with the V_{Ti}-$6V_O$ exhibiting a lifetime 130 ps longer than the isolated V_{Ti}. The positron lifetimes of cation divacancies connected with oxygen vacancies
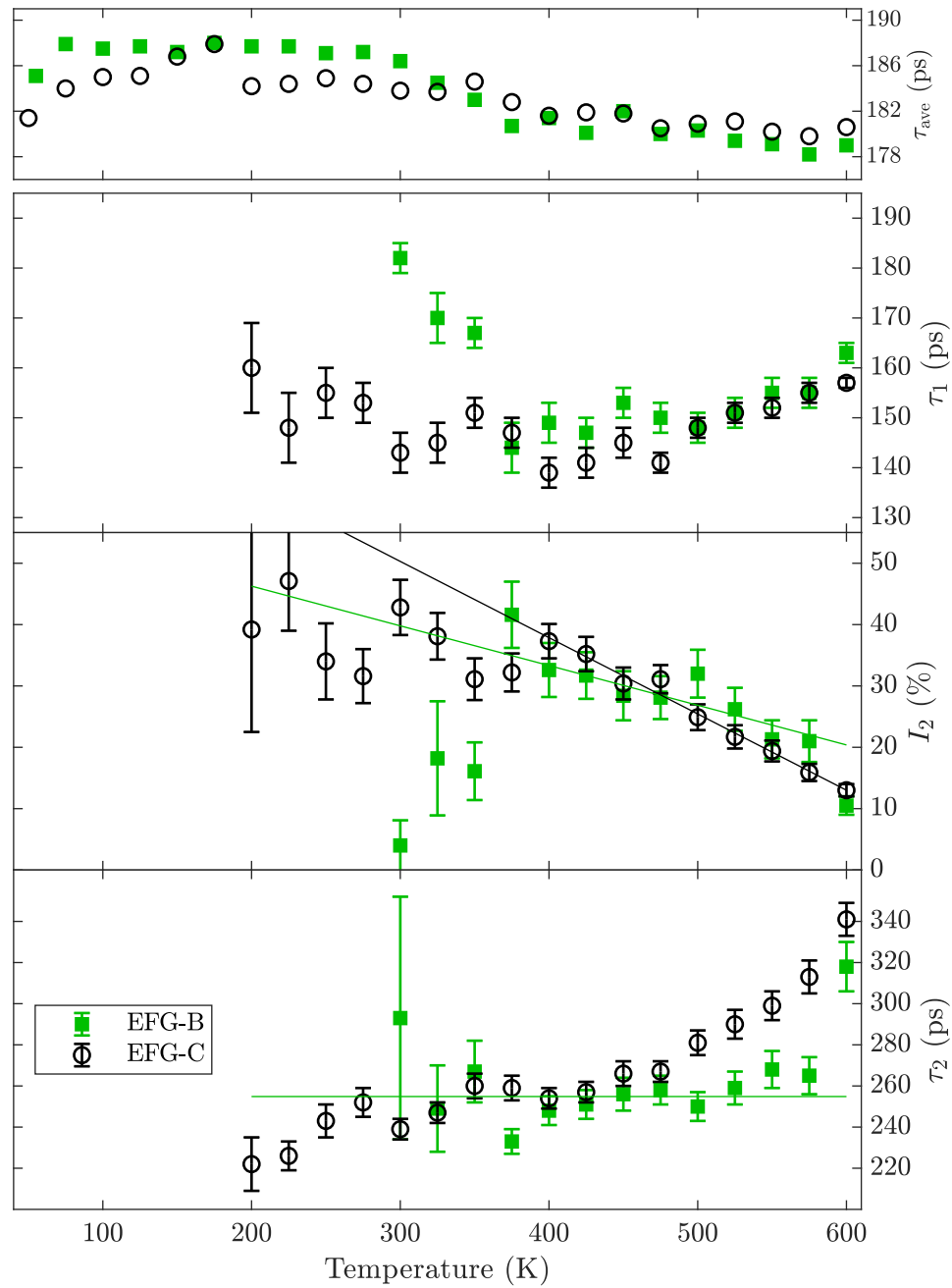
FIG. 4. The average lifetimes τ_{ave}, the decomposed lifetime components τ_1 and τ_2, and the intensity of the second component I_2 in samples EFG-B and EFG-C. The intensity of the first component is $1 - I_2$. An error weighted average of the τ_2 in EFG-B is shown $\tau = 255 \pm 15\,\mathrm{ps}$. Trendlines of the intensities of the second lifetime component I_2 illustrate the difference in behavior above $400\,\mathrm{K}$.

TABLE I. Positron lifetimes predicted with theoretical calculations.

Defect	Lifetime (ps)	Defect	Lifetime (ps)
lattice	128	V_{O}	no trapping
Ti_{Sr}	$\tau_{\text{B}} + 32 \ldots 42$	Sr_{Ti}	no trapping
Ti_{Sr}-V_{O}	$\tau_{\text{B}} + 40$	Sr_{Ti}-V_{O}	no trapping
V_{Sr}	$\tau_{\text{B}} + 105$	V_{Ti}	$\tau_{\text{B}} + 44$
V_{Sr}-V_{O}	$\tau_{\text{B}} + 107$	V_{Ti}-V_{O}	$\tau_{\text{B}} + 61$
V_{Sr}-$2V_{\text{O}}$	$\tau_{\text{B}} + 109$	V_{Ti}-$2V_{\text{O}}$	$\tau_{\text{B}} + 72$
V_{Sr}-$4V_{\text{O}}$	$\tau_{\text{B}} + 121$	V_{Ti}-$4V_{\text{O}}$	$\tau_{\text{B}} + 101$
V_{Sr}-$6V_{\text{O}}$	$\tau_{\text{B}} + 136$	V_{Ti}-$6V_{\text{O}}$	$\tau_{\text{B}} + 173$
$2V_{\text{Sr}}$-V_{O}	$\tau_{\text{B}} + 113$	$2V_{\text{Ti}}$-V_{O}	$\tau_{\text{B}} + 65$
$2V_{\text{Sr}}$-$4V_{\text{O}}$	$\tau_{\text{B}} + 136$	$2V_{\text{Ti}}$-$4V_{\text{O}}$	$\tau_{\text{B}} + 64$

are in the range of cation monovacancies decorated with V_{O}.

IV. DISCUSSION

A. Three vacancy-type defects

The saturation of the average positron lifetime below $300\,\text{K}$ in sample Cz-D indicates that all positrons annihilate as trapped at a vacancy-type defect with a positron lifetime of $185 \pm 5\,\text{ps}$. Above $300\,\text{K}$, this saturation trapping fades out and the average lifetime decreases reaching $165\,\text{ps}$ at $600\,\text{K}$ implying that the lifetime in SrTiO_3 lattice is at most $\tau_B \leq 165\,\text{ps}$, the shortest of the average positron lifetimes measured in this work.

In samples EFG-A1 and EFG-A2, the same vacancy defect with positron lifetime of $185 \pm 5\,\text{ps}$ is trapping all positrons below $150\,\text{K}$. At high temperatures, positron trapping to a vacancy defect with a positron lifetime of $\tau_D = 320 \pm 20\,\text{ps}$ increases. The defect responsible for the $320 \pm 20\,\text{ps}$ positron lifetime is present in samples EFG-A1 and EFG-A2 in different concentrations, as τ_{ave} and I_2 are slightly higher in EFG-A2. The $320 \pm 20\,\text{ps}$ lifetime component represents clearly only one defect as the extracted lifetime is constant for the whole decomposition temperature range ($>300\,\text{K}$) in both samples, and the two samples

with different defect concentrations give the same lifetime component (Fig.3).

The 185 ± 5 ps defect is trapping all positrons below 200 K also in samples EFG-B and EFG-C. At temperatures above 200 K, where the saturation trapping to this defect begins to roll off, the lifetime decomposition resolves two lifetime components. The constant value of τ_2 in EFG-B and the plateau in EFG-C suggest the presence of a 255 ± 15 ps defect-related lifetime (Fig. 4). The fact that the second lifetime component, τ_2, in sample EFG-C increases from 220 ps to above 300 ps is a "text book example" of multiple defect lifetimes being mixed into a single fitted lifetime component. The results suggest that all three observed vacancy defects contribute to τ_2. Below 300 K in sample EFG-C, τ_2 appears as a combination of 185 ± 5 ps (or at least shorter than 220 ps) and 255 ± 15 ps defect lifetimes, above 300 K the 185 ± 5 ps vacancy ceases to trap positrons, and above 400 K the positron trapping shifts from the 255 ± 15 ps vacancy towards the vacancy responsible for the positron lifetime of 320 ± 20 ps (or longer).

Altogether, at least three distinct vacancy-type defects were found to contribute to the positron annihilation data at temperatures above the observed saturation trapping to the 185 ± 5 ps defect. Fitting more than two lifetime components to the experimental data was not possible, for which the most likely reason is that the different components are too close to each other. Generally, the ratio of two lifetime components should be more than 1.5 for them to be separable in the fitting. This severely complicates the identification of the defects affecting the positron annihilation spectra. Further challenges in defect identification are imposed by the lack of a proper reference sample that could reliably be interpreted as producing the positron lifetime characterizing the SrTiO$_3$ lattice (τ_B).

As an example, we consider the highest-temperature data obtained in the sample EFG-A1. A simple assumption that at 600 K only the 320 ps defect would be trapping positrons would allow us to use the single-defect trapping model[37] for estimating the lifetime in SrTiO$_3$ lattice through $\tau_B = (\tau_1 \tau_2)/(\tau_1 + \tau_2 - \tau_{\mathrm{ave}})$. However, this gives a value of roughly 180 ps, which is obviously wrong as the lifetime in lattice must satisfy $\tau_B \lesssim 165$ ps (see Sec. III). The reason for the too large a value is the mixing of the 185 ps defect lifetime with τ_1 in the fitting.

In spite of all the complications generated by the large number of different vacancy-type defects in the samples, the above considerations also provide a possibility to make an estimate for positron lifetime in SrTiO$_3$ lattice. As the sample Cz-D appears to contain only the 185 ps defect, we can place a lower bound on τ_1 keeping in mind that it should not be

resolvable in the analysis. The "1.5 ratio rule" pointed out above implies that $\tau_1 \gtrsim 110$ ps, if $\tau_2 = 185$ ps (which is within the limits of the poor fitting result for Cz-D, see Sec. III). With the single defect model, this gives the estimate $\tau_B \gtrsim 155$ ps. Hence, we arrive at our estimate for the positron lifetime in SrTiO$_3$ lattice as $\tau_B \approx 155$ ps.

B. Temperature dependent trapping at the 185 ps vacancy defect

The clearest feature of the positron lifetime results, and common to all samples, is the saturation trapping at low temperatures at the defect with the positron lifetime of 185 ± 5 ps. However, the temperature behavior of the trapping to this defect is non-trivial. An increased trapping rate at low temperatures is usually interpreted as a fingerprint of negative defects for which the trapping coefficient is proportional to $T^{-1/2}$ (Ref. [38]). The temperature dependence of the trapping at the 185 ± 5 ps defect is significantly steeper. The results show that at low temperatures (<150 K in EFG-A1, EFG-A2 and EFG-C, <300 K in EFG-B and Cz-D), the 185 ± 5 ps vacancy traps all positrons, meaning that the positron trapping rate of the vacancy is significantly larger than any other trapping or annihilation rate. Above a sample-dependent temperature, the trapping rate drops rather dramatically taking into account the temperature range, resembling a $\sim T^{-3}$ dependence instead of $T^{-1/2}$.

This kind of stronger temperature dependence, where the trapping changes from a "strong-trapping" to essentially "no-trapping" regime when temperature is increased, suggests that positrons are able to escape (thermally) from the trap[9]. The onset of this type of effect at around 300-400 K corresponds to a defect binding energy of ~ 130 meV, and at around 150 K to a binding energy of ~ 70 meV[39–41]. It is important to note that these values correspond to states with a large radius of the trapped state and no increase in positron lifetime (compared to the lattice) is usually associated. The lifetime of the 185 ps defect is only ~ 30 ps longer than in the lattice, relying on the estimate in the present work. Hence, the open volume of defect is rather small resulting in a smaller-than usual binding energy (typically for vacancies 1 eV), and could at high temperatures allow positrons escaping the defect. Similar observations have been made for small substitutional impurities on the metal sublattice in ZnO and GaN[10,12], where the defects have vacancy character with strongly reduced open volume from the positron perspective. In the case where these low binding energies are associated with hydrogen-like Rydberg states around a

13

negative non-open volume defect (negative ion), observing two different binding energies for apparently the same defect could be interpreted as two different charges states, e.g., 2- and 3- (as the binding energy is proportional to Z^2)[40]. In the case of a neutral defect, a possible explanation is that the defect in question appears in slightly different atomic configurations, resulting in different binding energies without major changes to the lifetime. For defects on the Sr site, a similar effect could be brought by the coupling with one or two O vacancies (see Table I).

A similar faster-than-$T^{-1/2}$ decrease in trapping to the 185 ± 5 ps defect can also be seen in the temperature-resolved positron lifetime results published earlier[13]. In those results, the positron trapping to the 185 ± 5 ps defect is in saturation at low temperatures (below 100 K), and towards 293 K the average lifetime decreases to 165 ps. In principle, the temperature dependence in both our data and the data published in Ref. 13 could be explained by changes in the charge states of the defects (involving both negative/neutral and positive charge states, as the changes in trapping rates are several orders of magnitude) due the motion of the Fermi level with temperature. However, the number of free parameters in building such a model for explaining these results is significantly higher than in the "shallow vacancy model" described above. Hence, we refrain from discussing this possibility in more detail.

C. Defect identities

Saturation trapping to a defect occurs in practice when the trapping rate κ_D to this particular defect exceeds the annihilation rate in the lattice by two orders of magnitude: $\kappa_D \geq 100\tau_B^{-1}$. The trapping rate is related to the defect concentration c_D through $\kappa_D = \mu_D c_D$, where μ_D is the trapping coefficient. For negatively charged defects $\mu_D \simeq 5 \times 10^{15}$ s^{-1} at 150 K, and for neutral defects $\mu_D \simeq 1 \times 10^{15}$ s^{-1} irrespective of temperature. Hence, the saturation trapping condition can be expressed as $c_D \geq 100\ldots500$ ppm, corresponding to $\sim 1\ldots5 \times 10^{19}$ cm^{-3} in SrTiO$_3$. As a consequence, the 185 ps defect is extremely abundant in all the studied samples. As this defect lifetime is the most frequently observed defect lifetime in literature[13–20], identifying this defect is of great importance for understanding the properties of SrTiO$_3$. At the highest measurement temperatures, where the trapping to this defect has vanished to a large extent, the average positron lifetime measured in the

EFG samples is still closer to $\tau_B \approx 155$ ps than to the respective defect lifetime of 255 ps or 320 ps found in the sample, allowing us to estimate that the concentrations of these defects are at most in the low-10^{17} cm^{-3} range.

Detailed identification of vacancy-type defects based on positron lifetime experiments is at its best when experimental and calculated lifetimes can be reliably compared. As the predictive power of the state-of-the-art theoretical calculations in terms of the absolute scale of positron lifetimes is low due to the different choices of approximations resulting in a wide range of, e.g., lifetimes in SrTiO$_3$ lattice, reliable comparison requires a common point of reference for experiment and theory. If a sample producing a single component in the lifetime spectrum can be reliably identified as producing the lifetime in the SrTiO$_3$ lattice, the situation is optimal. However, in the case of SrTiO$_3$ this is not the case. There are a few reports where a single lifetime of 135-140 ps is reported and interpreted as the lifetime in SrTiO$_3$ lattice[14,15,21]. These values have been obtained by performing the experiments in a single sample at room temperature with Kapton-encapsulated Na sources that produce very strong source components in the spectra, increasing the uncertainty of the fitting procedures. Also, the fitting procedures (e.g., source corrections) have not been described in detail in these reports, making the comparison to our results difficult. A careful and systematic study[13], where several samples were studied as a function of temperature with different types of positron sources, reports an estimated lifetime in SrTiO$_3$ lattice of $\tau_B \approx 155$ ps. This coincides with our interpretation (see Sec. IV A). It should be noted, however, that both our interpretation and that in Ref. 13 rely on experiments, analysis and interpretation of lifetime spectra containing more than one component. Further investigations are required to obtain better insight into this matter. In the following analysis, we use $\tau_B \approx 155$ ps as the lifetime in lattice in our experiments.

The theoretical calculations (see Table I) show that V_O does not trap positrons, and that the simple elemental vacancies V_{Sr} and V_{Ti} should have positron lifetimes ~ 105 ps and ~ 45 ps longer than in the lattice, respectively. In our experiments, this would translate to ~ 260 ps for V_{Sr} and ~ 200 ps for V_{Ti}. The only simple defect producing a lifetime close to ~ 30 ps longer than in the lattice in the calculations, corresponding to 185 ps in the experiments, is the Ti$_{Sr}$ antisite. Hence, we identify the defect producing the 185 ps lifetime component as the Ti$_{Sr}$ antisite. As the effect of adding one or more V_O to Sr-site open volume defects is minimal, it is possible that the observed Ti$_{Sr}$ antisite defects are coupled

with O vacancies.

This identification is in line with several other findings. First, the samples studied in this work were grown from stoichiometric melts, but due to the evaporation of SrO(g) a slight TiO_2 excess in the melt can be expected at increased growth durations,[42] making it unlikely that the most dominant defects would occur as vacancies on the Ti sublattice. In fact, theoretical calculations predict that V_{Sr} are more favorable than V_{Ti} already at stoichiometric Sr/Ti conditions[3]. Second, theoretical calculations also suggest that Ti_{Sr} antisites are energetically favorable in TiO_2-rich $SrTiO_3$, and in neutral charge state in the upper half of the bandgap[5,8]. Third, the existence of Ti_{Sr} antisites has been experimentally observed with scanning transmission electron microscopy (STEM) in heteroepitaxial $SrTiO_3$ thin films,[7] suggesting that they can be present in $SrTiO_3$ in large concentrations. Finally, $SrTiO_3$ tends to be oxygen deficient[43] - hence the presence of a high concentration of O vacancies is natural. Theoretical calculations also predict that forming of a Ti_{Sr}-V_O pair is energetically favorable[5,6]. We also suggest that the 185 ps lifetime observed in many earlier reports[13–20], based on measurements in commercial $SrTiO_3$ crystals grown by the Verneuil method in addition to Cz and EFG methods, is also the Ti_{Sr} antisite instead of the V_{Ti} proposed in those reports, as Verneuil growth tends to lead to material rich in Ti as well[44].

Following the above reasoning and comparing with Table I, the defect producing the experimental 255 ± 15 ps positron lifetime is interpreted as the Sr vacancy V_{Sr} ($\tau_B + 95 \pm 15$ ps), possibly coupled with one or two O vacancies. The experimental results also point at a negative charge state in the case of the 255 ± 15 ps vacancy as the intensity related to this lifetime decreases in both samples above 400 K (see Fig. 4), in line with the negative charge states predicted for V_{Sr}[3]. Similarly, the defect responsible for the experimental 320 ± 20 ps is interpreted as one or more Sr vacancies clustered with multiple O vacancies. This defect appears neutral in the experiments, as typically expected for large cation-oxygen vacancy complexes in oxides. Interestingly, nanovoids formed by multiple Sr-O divacancies have been previously observed in top-seeded solution grown $SrTiO_3$ crystals[45].

The identification of the defects as suggested above is in line with the differences in the growth conditions of the single crystal $SrTiO_3$ samples. Compared to EFG-A1 and EFG-A2, the oxygen concentration during growth and post-growth processes was significantly higher for the samples EFG-B and EFG-C. The latter samples are the ones with Sr vacancies, while the former contain the large Sr vacancy - O vacancy clusters (with multiple O vacancies).

This is reasonable as the samples EFG-A1/2 also show clear indications of oxygen deficiencies through to the blue-black coloration[43]. The other samples are yellowish (EFG) or yellowish-brownish (Czochralski), which clearly shows that the back-diffusion of oxygen took place. It is worth to mention that the growing crystals are deficient in oxygen at temperatures very close to the melting point and only a sufficiently high oxygen partial pressure will allow back-diffusion of oxygen at lower temperatures. For the Czochralski grown crystal (sample Cz-D) we assume that the high pulling rates between 20 and 70 mm/h (see also Ref. 42 crystal C2) compared to the EFG crystals (between 1 and 7 mm/h) inhibited the formation of Sr vacancies in the bulk, since the more SrO is available during growth, the less likely is the formation of this type of defect[8]. The low formation enthalpies of Ti_{Sr} antisites could explain their persistence under these harsh conditions during the Czochralski growth. Finally, we wish to point out that time-dependent factors both during growth and post-growth processes can play an important role in the formation and/or stabilization of specific kinds of defects.

V. CONCLUSIONS

We performed temperature-dependent positron lifetime measurements on $SrTiO_3$ single crystals grown in different conditions. Three different vacancy-type defects were found in the samples with positron lifetimes 185 ± 5 ps, 255 ± 15 ps and 320 ± 20 ps. The 185 ± 5 ps defect is present in all the measured samples at very high concentrations (at least $\sim 10^{19}$ cm^{-3}). The presence of the other two defects depends on the growth conditions, and their concentrations are at most in the low-10^{17} cm^{-3} range. Based on detailed analysis of the temperature-dependent positron data and comparison to state-of-the-art theoretical calculations, we suggest that the 185 ± 5 ps defect is the Ti_{Sr} antisite, possibly coupled with one or two O vacancies. The defects with longer lifetimes are identified as Sr vacancies in the negative charge state (255 ± 15 ps) and as neutral clusters containing multiple Sr and O vacancies (320 ± 20 ps). We also suggest that the abundant Ti_{Sr} antisite related defect is responsible for the ~ 185 ps lifetime component reported in earlier studies[13–20] in $SrTiO_3$ single crystals as well.

Our work highlights the importance of being able to reliably resolve lifetime components in the positron lifetime spectrum, and of having a reliable estimate of the positron lifetime

in the lattice, if defect identification is aimed for. This cannot be achieved by performing a single experiment on a single sample at a single temperature (typically room temperature). The mixing of different defect-related lifetime components in the analysis in $SrTiO_3$ is an important issue, and complicates the analysis of the data, as showed in the case of each of the studied samples. Performing experiments across a wide temperature range does not prevent this mixing from taking place, but helps in recognizing its occurrence and in providing indisputable evidence of positrons annihilating as trapped at defects. Another complication is the identification of the proper reference lifetime in the $SrTiO_3$ lattice for accurate quantification of the changes caused by the defects. These issues require further detailed investigations in order to reliably identify the point defects governing the properties of $SrTiO_3$ crystals.

ACKNOWLEDGMENTS

The data that support the findings of this study are available from the corresponding author upon reasonable request.

REFERENCES

[1]K. van Benthem, C. Elser, and R. H. French, "Bulk electronic structure of $SrTiO_3$: Experiment and theory," Journal of Applied Physics **90**, 6156–6164 (2001), https://doi.org/10.1063/1.1415766.

[2]Y.-Y. Pai, A. Tylan-Tyler, P. Irvin, and J. Levy, "Physics of $SrTiO_3$-based heterostructures and nanostructures: a review," Reports on Progress in Physics **81**, 036503 (2018).

[3]A. Janotti, J. B. Varley, M. Choi, and C. G. Van de Walle, "Vacancies and small polarons in $SrTiO_3$," Physical Review B **90**, 085202 (2014).

[4]D. Lee, H. Lu, Y. Gu, S.-Y. Choi, S.-D. Li, S. Ryu, T. Paudel, K. Song, E. Mikheev,

S. Lee, *et al.*, "Emergence of room-temperature ferroelectricity at reduced dimensions," Science **349**, 1314–1317 (2015).

[5] M. Choi, F. Oba, and I. Tanaka, "Role of Ti antisite-like defects in srtio$_3$," Phys. Rev. Lett. **103**, 185502 (2009).

[6] K. Klyukin and V. Alexandrov, "Effect of intrinsic point defects on ferroelectric polarization behavior of SrTiO$_3$," Phys. Rev. B **95**, 035301 (2017).

[7] F. Yang, Q. Zhang, Z. Yang, J. Gu, Y. Liang, W. Li, W. Wang, K. Jin, L. Gu, and J. Guo, "Room-temperature ferroelectricity of SrTiO$_3$ films modulated by cation concentration," Applied Physics Letters **107**, 082904 (2015), https://doi.org/10.1063/1.4929610.

[8] B. Liu, V. R. Cooper, H. Xu, H. Xiao, Y. Zhang, and W. J. Weber, "Composition dependent intrinsic defect structures in SrTiO$_3$," Phys. Chem. Chem. Phys. **16**, 15590–15596 (2014).

[9] F. Tuomisto and I. Makkonen, "Defect identification in semiconductors with positron annihilation: Experiment and theory," Reviews of Modern Physics **85**, 1583 (2013).

[10] K. M. Johansen, A. Zubiaga, I. Makkonen, F. Tuomisto, P. T. Neuvonen, K. E. Knutsen, E. V. Monakhov, A. Yu. Kuznetsov, and B. G. Svensson, "Identification of substitutional Li in n-type ZnO and its role as an acceptor," Physical Review B **83**, 245208 (2011).

[11] K. M. Johansen, A. Zubiaga, F. Tuomisto, E. V. Monakhov, A. Yu. Kuznetsov, and B. G. Svensson, "H passivation of Li on Zn-site in ZnO: Positron annihilation spectroscopy and secondary ion mass spectrometry," Physical Review B **84**, 115203 (2011).

[12] F. Tuomisto, V. Prozheeva, I. Makkonen, T. H. Myers, M. Bockowski, and H. Teisseyre, "Amphoteric Be in GaN: Experimental evidence for switching between substitutional and interstitial lattice sites," Physical Review Letters **119**, 196404 (2017).

[13] R. A. Mackie, S. Singh, J. Laverock, S. B. Dugdale, and D. J. Keeble, "Vacancy defect positron lifetimes in strontium titanate," Phys. Rev. B **79**, 014102 (2009).

[14] A. Uedono, K. Shimoyama, M. Kiyohara, Z. Q. Chen, K. Yamabe, T. Ohdaira, R. Suzuki, and T. Mikado, "Vacancy-type defects in BaTiO$_3$/SrTiO$_3$ structures probed by monoenergetic positron beams," Journal of Applied Physics **91**, 5307–5312 (2002), https://doi.org/10.1063/1.1462852.

[15] A. Uedono, K. Shimayama, M. Kiyohara, Z. Q. Chen, and K. Yamabe, "Study of oxygen vacancies in SrTiO$_3$ by positron annihilation," Journal of Applied Physics **92**, 2697–2702 (2002), https://doi.org/10.1063/1.1498889.
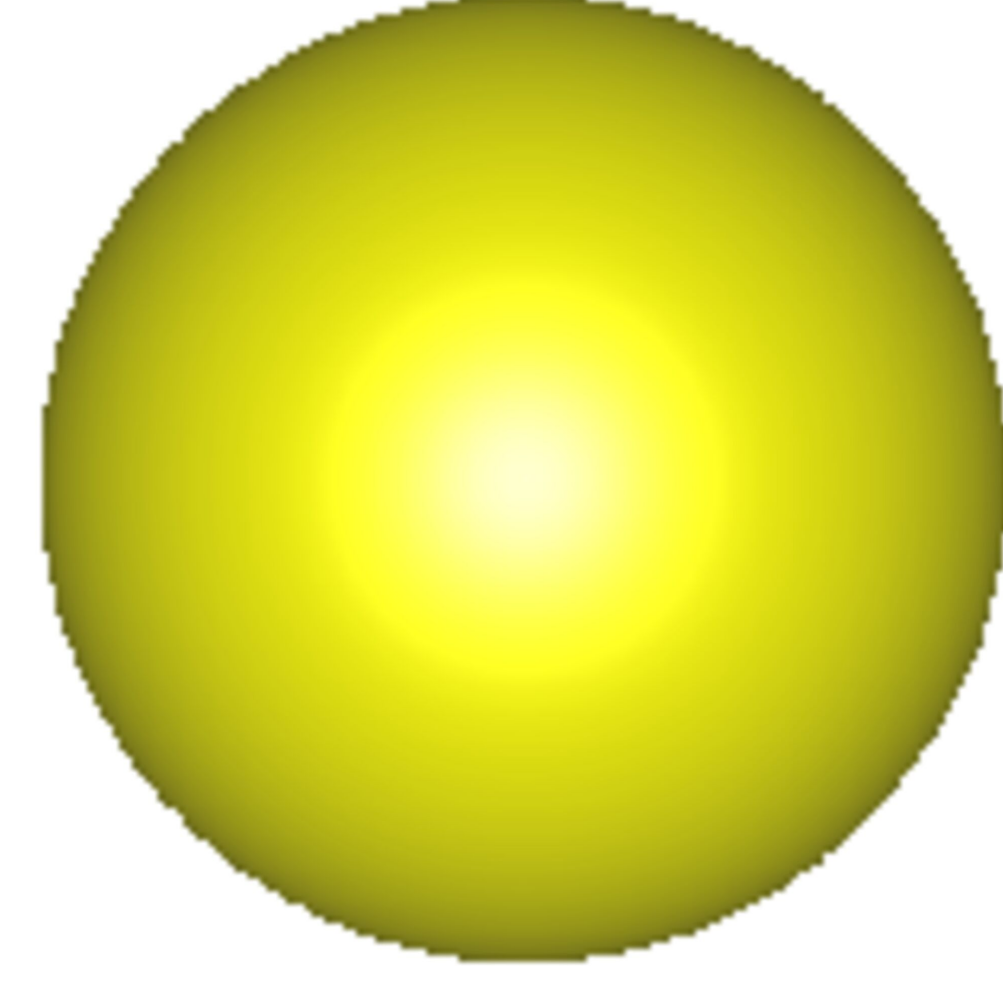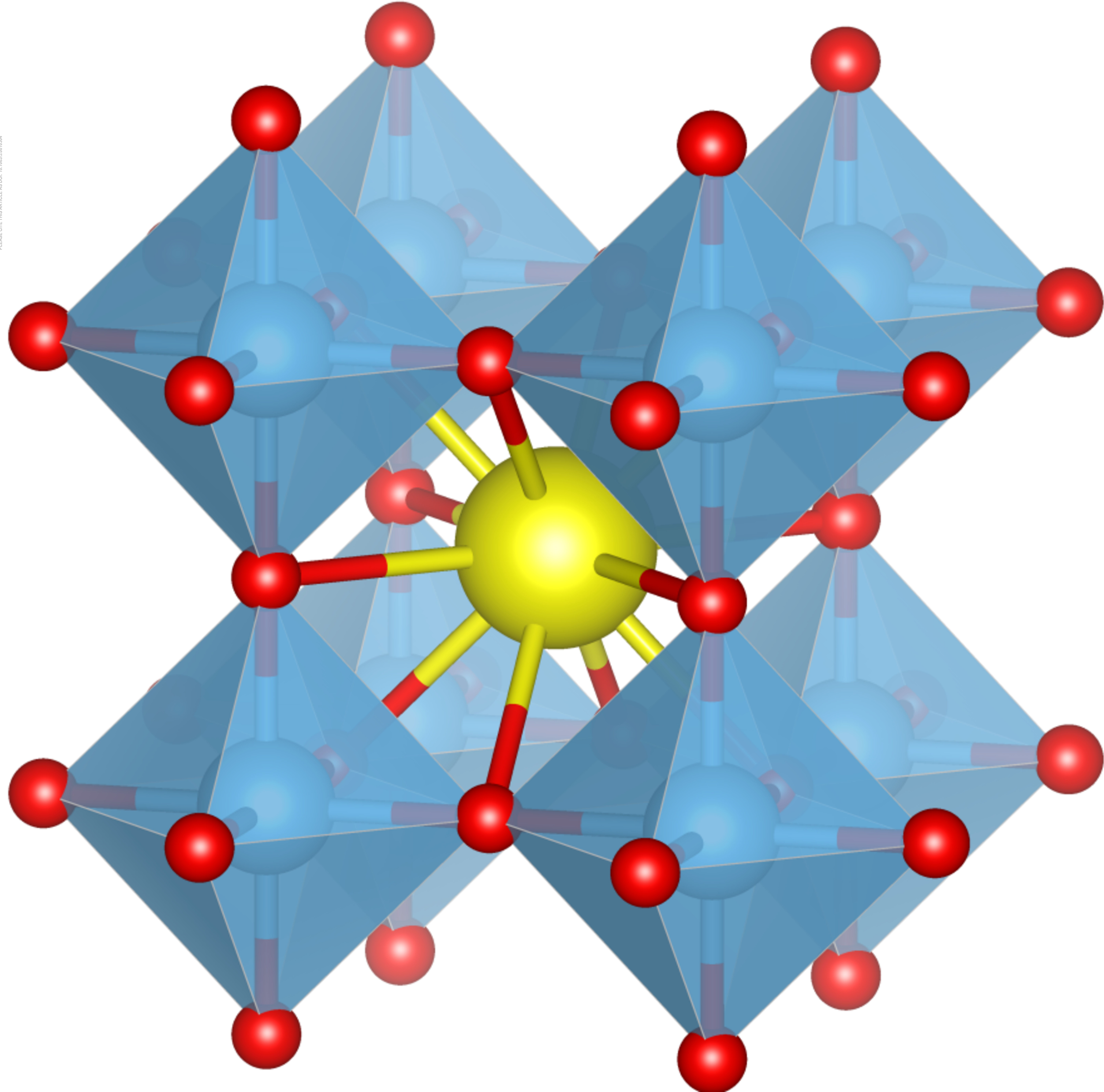
[16]D. J. Keeble, S. Wicklein, R. Dittmann, L. Ravelli, R. A. Mackie, and W. Egger, "Identification of a- and b-site cation vacancy defects in perovskite oxide thin films," Phys. Rev. Lett. **105**, 226102 (2010).

[17]M. C. Tarun, F. A. Selim, and M. D. McCluskey, "Persistent photoconductivity in strontium titanate," Phys. Rev. Lett. **111**, 187403 (2013).

[18]D. J. Keeble, R. A. Mackie, W. Egger, B. Löwe, P. Pikart, C. Hugenschmidt, and T. J. Jackson, "Identification of vacancy defects in a thin film perovskite oxide," Phys. Rev. B **81**, 064102 (2010).

[19]F. Selim, D. Winarski, C. Varney, M. Tarun, J. Ji, and M. McCluskey, "Generation and characterization of point defects in $SrTiO_3$ and $Y_3Al_5O_{12}$," Results in Physics **5**, 28 – 31 (2015).

[20]P. Saadatkia, P. Stepanov, and F. A. Selim, "Photoconductivity of bulk $SrTiO_3$ single crystals at room temperature," Materials Research Express **5**, 016202 (2018).

[21]A. S. Hamid, A. Uedono, T. Chikyow, K. Uwe, K. Mochizuki, and S. Kawaminami, "Vacancy-type defects and electronic structure of perovskite-oxide $SrTiO_3$ from positron annihilation," physica status solidi (a) **203**, 300–305 (2006).

[22]I. Makkonen, M. Hakala, and M. J. Puska, "Modeling the momentum distributions of annihilating electron-positron pairs in solids," Phys. Rev. B **73**, 035103 (2006).

[23]J. Wiktor, G. Jomard, and M. Torrent, "Two-component density functional theory within the projector augmented-wave approach: Accurate and self-consistent computations of positron lifetimes and momentum distributions," Phys. Rev. B **92**, 125113 (2015).

[24]S. Ishibashi and A. Uedono, "Computational studies of positron states and annihilation parameters in semiconductors – vacancy-type defects in group-III nitrides –," Journal of Physics: Conference Series **674**, 012020 (2016).

[25]I. Makkonen, E. Korhonen, V. Prozheeva, and F. Tuomisto, "Identification of vacancy defect complexes in transparent semiconducting oxides ZnO, In_2O_3 and SnO_2," J. Phys.: Cond. Matt. **28**, 224002 (2016).

[26]C. Guguschev, Z. Galazka, D. J. Kok, U. Juda, A. Kwasniewski, and R. Uecker, "Growth of $SrTiO_3$ bulk single crystals using edge-defined film-fed growth and the czochralski methods," CrystEngComm **17**, 4662–4668 (2015).

[27]J. P. Perdew and A. Zunger, "Self-interaction correction to density-functional approximations for many-electron systems," Phys. Rev. B **23**, 5048–5079 (1981).

[28]P. E. Blöchl, "Projector augmented-wave method," Phys. Rev. B **50**, 17953–17979 (1994).

[29]G. Kresse and J. Furthmüller", "Efficiency of ab-initio total energy calculations for metals and semiconductors using a plane-wave basis set," Computational Materials Science **6**, 15 – 50 (1996).

[30]G. Kresse and J. Furthmüller, "Efficient iterative schemes for ab initio total-energy calculations using a plane-wave basis set," Phys. Rev. B **54**, 11169–11186 (1996).

[31]G. Kresse and D. Joubert, "From ultrasoft pseudopotentials to the projector augmented-wave method," Phys. Rev. B **59**, 1758–1775 (1999).

[32]E. Boroński and R. M. Nieminen, "Electron-positron density-functional theory," Phys. Rev. B **34**, 3820–3831 (1986).

[33]M. J. Puska, A. P. Seitsonen, and R. M. Nieminen, "Electron-positron Car-Parrinello methods: Self-consistent treatment of charge densities and ionic relaxations," Phys. Rev. B **52**, 10947–10961 (1995).

[34]M. J. Puska and R. M. Nieminen, "Defect spectroscopy with positrons: a general calculational method," Journal of Physics F: Metal Physics **13**, 333–346 (1983).

[35]M. J. Puska and R. M. Nieminen, "Theory of positrons in solids and on solid surfaces," Rev. Mod. Phys. **66**, 841–897 (1994).

[36]K. Momma and F. Izumi, "*VESTA3* for three-dimensional visualization of crystal, volumetric and morphology data," Journal of Applied Crystallography **44**, 1272–1276 (2011).

[37]P. Hautojärvi and C. Corbel, "Positron spectroscopy of defects in metals and semiconductors," Positron spectroscopy of solids **125**, 491–532 (1995).

[38]M. J. Puska, C. Corbel, and R. M. Nieminen, "Positron trapping in semiconductors," Phys. Rev. B **41**, 9980–9993 (1990).

[39]K. Saarinen, T. Laine, S. Kuisma, J. Nissilä, P. Hautojärvi, L. Dobrzynski, J. M. Baranowski, K. Pakula, R. Stepniewski, M. Wojdak, A. Wysmolek, T. Suski, M. Leszczynski, I. Grzegory, and S. Porowski, "Observation of native Ga vacancies in GaN by positron annihilation," Phys. Rev. Lett. **79**, 3030–3033 (1997).

[40]F. Tuomisto, V. Ranki, D. C. Look, and G. C. Farlow, "Introduction and recovery of Ga and N sublattice defects in electron-irradiated GaN," Phys. Rev. B **76**, 165207 (2007).

[41]J.-M. Mäki, I. Makkonen, F. Tuomisto, A. Karjalainen, S. Suihkonen, J. Räisänen, T. Y. Chemekova, and Y. N. Makarov, "Identification of the V_{al}-o$_n$ defect complex in AlN single crystals," Phys. Rev. B **84**, 081204 (2011).
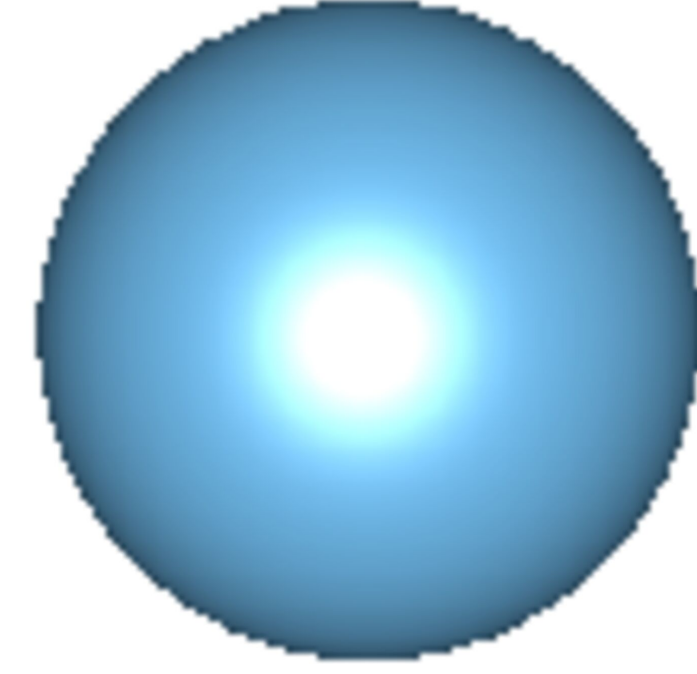
[42]C. Guguschev, Z. Galazka, D. J. Kok, U. Juda, A. Kwasniewski, and R. Uecker, "Growth of SrTiO$_3$ bulk single crystals using edge-defined film-fed growth and the Czochralski methods," CrystEngComm **17**, 4662–4668 (2015).

[43]C. Guguschev, D. J. Kok, Z. Galazka, D. Klimm, R. Uecker, R. Bertram, M. Naumann, U. Juda, A. Kwasniewski, and M. Bickermann, "Influence of oxygen partial pressure on SrTiO$_3$ bulk crystal growth from non-stoichiometric melts," CrystEngComm **17**, 3224–3234 (2015).

[44]Y. Tateno, K. Endo, S. Arisawa, A.-M. Vlaicu, L. Nedelcu, N. Preda, M. Secu, R. Iordanescu, A. C. Kuncser, and P. Badica, "Growth of SrTiO$_3$ single crystals with a diameter of about 30 mm by the Verneuil method," Crystal Growth & Design **19**, 604–612 (2019), https://doi.org/10.1021/acs.cgd.8b01004.

[45]D. J. Kok, C. Guguschev, T. Markurt, M. Niu, R. Bertram, M. Albrecht, and K. Irmscher, "Origin of brown coloration in top-seeded solution grown SrTiO$_3$ crystals," CrystEngComm **18**, 4580 (2016).
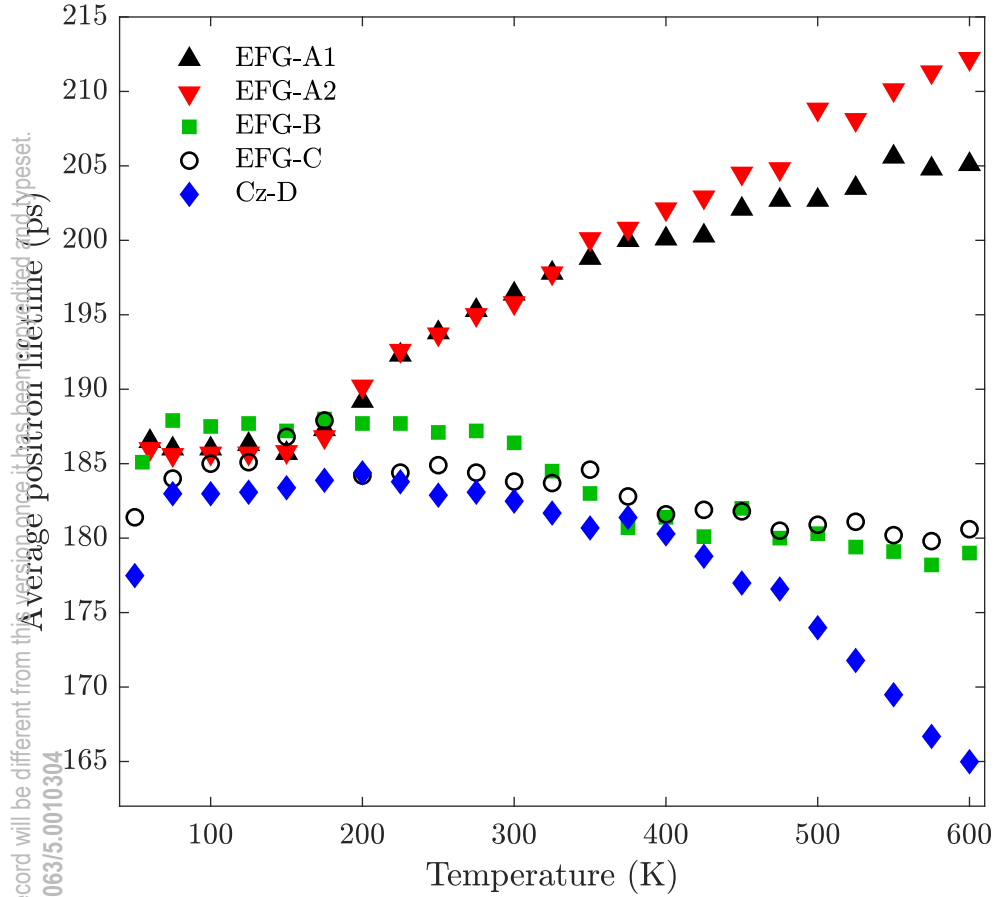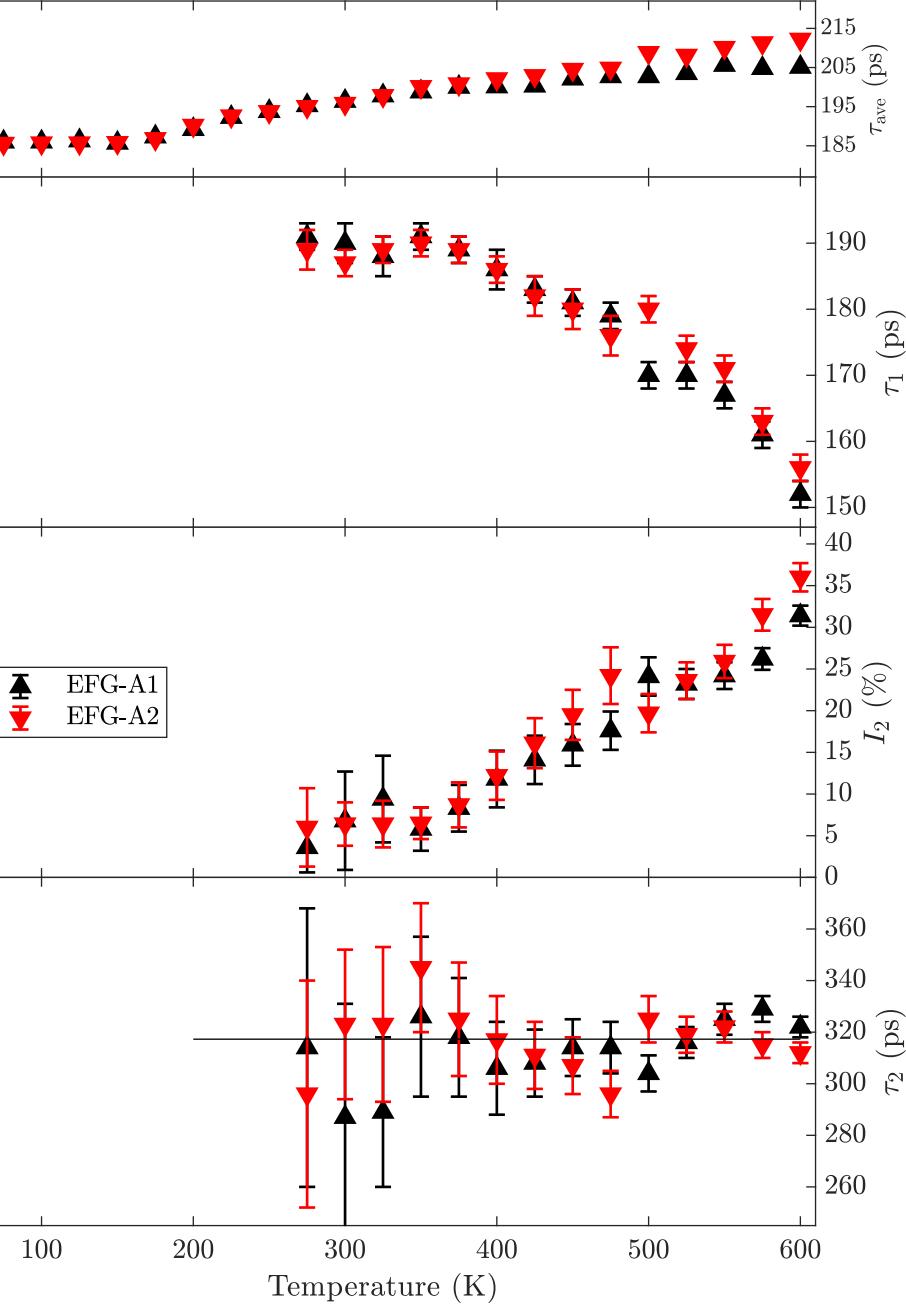
Sr

Ti

O